

L_1 Trend Filtering: A Modern Statistical Tool for Time-Domain Astronomy and Astronomical Spectroscopy

Collin A. Politsch,^{1,2*} Jessi Cisewski-Kehe,³ Rupert A. C. Croft,^{4,5}
and Larry Wasserman^{1,2,5}

¹ Department of Statistics & Data Science, Carnegie Mellon University, Pittsburgh, PA 15213

² Machine Learning Department, Carnegie Mellon University, Pittsburgh, PA 15213

³ Department of Statistics and Data Science, Yale University, New Haven, CT 06520

⁴ Department of Physics, Carnegie Mellon University, Pittsburgh, PA 15213

⁵ McWilliams Center for Cosmology, Carnegie Mellon University, Pittsburgh, PA 15213

Accepted XXX. Received YYY; in original form 2019 August 19

ABSTRACT

The problem of estimating a one-dimensional signal possessing mixed degrees of smoothness is ubiquitous in time-domain astronomy and astronomical spectroscopy. For example, in the time domain, an astronomical object may exhibit a smoothly varying intensity that is occasionally interrupted by abrupt dips or spikes. Likewise, in the spectroscopic setting, a noiseless spectrum typically contains intervals of relative smoothness mixed with localized higher frequency components such as emission peaks and absorption lines. In this work, we present L_1 trend filtering (Steidl et al.; Kim et al.), a modern nonparametric statistical tool that yields significant improvements in this broad problem space of estimating *spatially heterogeneous* signals. When the underlying signal is spatially heterogeneous, the L_1 trend filter has been shown to be strictly superior to any estimator that is a linear combination of the observed data, including smoothing splines, kernels, and Gaussian processes. Moreover, the L_1 trend filter does not require the restrictive setup of wavelets — the definitive classical approach for modeling spatially heterogeneous signals.

In the spirit of illustrating the wide applicability of L_1 trend filtering, we briefly demonstrate its utility on several relevant astrophysical data sets: two Kepler light curves (an exoplanet transit and an eclipsing binary system), a Palomar Transient Factory supernova light curve, and an SDSS galaxy spectrum. Furthermore, we present a more rigorous analysis of the Lyman-alpha forest of SDSS quasar spectra — a standard cosmological tool for probing the large-scale structure of the high redshift intergalactic medium.

Key words: Methods: statistical, planets and satellites: detection, stars: binaries: eclipsing, supernovae: general, techniques: spectroscopic, cosmology: observations

1 INTRODUCTION

Many astronomical observations produce one-dimensional data with unknown or varying degrees of smoothness. These include data from time-domain astronomy, where transient events such as supernovae can show light curve variations on timescales ranging from seconds to years (e.g., Dimitriadis et al. 2017; Tolstov et al. 2019). Similarly, in astronomical spectroscopy, with wavelength (or frequency) as the indepen-

dent variable, sharp absorption or emission line features can be present alongside smoothly varying black body or other continuum radiation (see e.g., Tennyson 2019). In each of these general settings, we observe a signal plus noise and would like to estimate the underlying signal in a nonparametric (i.e. model-independent) but well-specified fashion. Commonly used nonparametric techniques include smoothing with a kernel (e.g., B. Hall et al. 2002), fitting a spline (e.g., Dhawan et al. 2015), and wavelet decompositions (e.g., Fligge & Solanki 1997; Golikhou & Butler 2014). In order to deal with heterogeneous degrees of smoothness present in the

* E-mail: capolitsch@cmu.edu

signal, kernels and splines require careful modifications, e.g. locally varying the kernel bandwidth and irregularly varying the spline knot locations and order (e.g., Francis et al. 1991; Selsing et al. 2016), leading to increased complexity. Further, while wavelets naturally adapt to heterogeneous degrees of smoothness, they require restrictive assumptions about the data, e.g. equal-spacing and sample size equal to a power of two. In this paper we introduce L_1 trend filtering (Steidl et al. 2006; Kim et al. 2009; Tibshirani 2014), a method which is new to the astronomical literature and has promise for dealing with these areas of data analysis.

Before formally introducing L_1 trend filtering, we first give some background to our primary example application—one taken from astronomical spectroscopy. The Lyman-alpha ($\text{Ly}\alpha$) forest is the name given to the absorption features seen in quasar spectra which are caused by neutral hydrogen in the intergalactic medium between a quasar and an observer. When emitted from an accretion disk close to the central black hole, the light from the quasar has a relatively smooth spectrum—a continuum—caused by the summed black body emission of gas with different temperatures at different disk radii (Osterbrock & Ferland 2006). Emission lines are also seen, and their intensities and line ratios supply information on the physical conditions in the line emitting gas. At least twenty broad emission lines, broadened by high velocities and temperatures can be measured in a single AGN, along with a similar number of narrow lines from colder gas (Marziani et al. 1996). The emitted spectrum therefore already consists of a superposition of components with varying degrees of smoothness. The $\text{Ly}\alpha$ forest arises when this spectrum is further processed with the addition of absorption lines. Light moving towards the observer is redshifted into resonance with the $\text{Ly}\alpha$ transition of neutral hydrogen, and the strength of absorption features is dictated by the densities of intergalactic material along the line of sight (Rauch 1998). The smoothness of the absorption lines varies depending on the gas pressure, and thermal doppler broadening (Gnedin & Hui 1998; Peebles et al. 2010). Sharper absorption features, metal lines, are also caused by other intergalactic species, such as CIV, OVI and MgII (Hellsten et al. 1998; Pieri et al. 2010). The usefulness of the $\text{Ly}\alpha$ forest as a cosmological probe (e.g., Palanque-Delabrouille et al. 2015) stems from its relationship to the matter density field in the Universe, effectively mapping out structure along each observer-quasar line of sight (e.g., Croft et al. 1997; Lee et al. 2014). In order to extract this information from noisy spectra and separate it from other components, it is useful to have a method which can deal with the complexities outlined above, i.e. one that can naturally adapt to the variations in smoothness without extensive tuning.

L_1 trend filtering was independently proposed in the computer vision literature (Steidl et al. 2006) and the applied mathematics literature (Kim et al. 2009), and has recently gained popularity in the statistical and machine learning literature, most notably with Tibshirani (2014), Ramdas & Tibshirani (2016), and Wang et al. (2016). For any given integer $k \geq 0$, the k th order L_1 trend filter is a one-dimensional piecewise polynomial of order $k \in \{0, 1, 2, \dots\}$ with knots automatically selected at a sparse subset of the observed inputs. The automatic knot selection in itself is significant because it renders obsolete piecewise polynomial and regression spline estimation procedures with knot selec-

tion done by eye or exhaustive search. The L_1 trend filter is obtained by minimizing a penalized least-squares criterion, with the penalization being on the summed absolute values of a discrete approximation of the estimator's $(k+1)$ st derivative at the knots. For this reason, for orders $k = 1$ and $k = 3$, the L_1 trend filter can be thought of as the L_1 analog to the classical (L_2 -penalized) linear and cubic smoothing splines, respectively. Here, the use of the L_1 penalty grants the estimator superior local adaptivity that leads to its optimality for estimating spatially heterogeneous signals. Additionally, unlike smoothing splines, the L_1 trend filter is well-defined for every order $k \in \{0, 1, 2, \dots\}$. A number of other key results were established in Tibshirani (2014). Namely,

- (1) For orders $k = 0, 1$ the L_1 trend filter is in fact a spline and exactly equal to a k th order locally adaptive regression spline (Mammen & van de Geer 1997), but comes at far less computational cost— $O(n^{1.5})$ versus $O(n^3)$;
- (2) For orders $k \geq 2$, the L_1 trend filter is a piecewise polynomial of order k , but possesses small discontinuities in lower order derivatives at the knots and thus is not quite a spline;
- (3) For any order $k \geq 0$, over a large space of functions containing both spatially homogeneous and heterogeneous signals, the L_1 trend filter converges to the true signal (in terms of mean-squared error) at the minimax rate.

The term *minimax* refers to a popular statistical concept for benchmarking the performance of an estimator, wherein the *minimax rate* is the gold standard. Specifically, the minimax rate is the fastest rate (in terms of the sample size) at which the worst-case error of an estimator can converge to zero. Donoho & Johnstone (1998) showed that the minimax rate is not achievable by any linear smoother, i.e. any estimator that is a linear combination of the observed data, when estimating spatially heterogeneous signals. To name a few, the linear smoother class includes popular methods such as smoothing splines, regression splines, polynomials, kernels, local polynomials, and Gaussian processes. Wavelets possess the minimax rate but require much more restrictive assumptions than L_1 trend filtering, e.g. equally-spaced inputs, sample size being a power of 2, and boundary conditions on the signal. The L_1 trend filter has a generalized lasso form; consequently, a number of other key properties follow directly from generalized lasso literature (Tibshirani & Taylor 2011; Tibshirani & Taylor 2012).

L_1 trend filtering software is available online across various platforms. The L_1 penalty makes the minimization criterion non-differentiable, but it is strictly convex, and a number of different algorithmic implementations are available for solving it in nearly linear time (with an $O(n^{1.5})$ computational complexity in the worst case). In this work we utilize the alternating direction method of multipliers (ADMM) algorithm of Ramdas & Tibshirani (2016), for which implementations are available in R and C¹, as well as Julia². For the primal-dual interior point method of Kim et al. (2009),

¹ <https://github.com/glmgen>

² <https://github.com/JuliaStats/Lasso.jl>

implementations are available in Matlab and C³, as well as wrappers for Python⁴ and R⁵.

The layout of the paper is as follows. In Section 2 we provide an introduction to L_1 trend filtering. In Section 3 we demonstrate L_1 trend filtering on four astrophysical data sets: two light curves from NASA’s Kepler mission, a Palomar Transient factory supernova light curve, and a galaxy spectrum from the Baryon Oscillation Spectroscopic Survey (BOSS; Dawson et al. 2013) of the Sloan Digital Sky Survey (SDSS; York et al. 2000). In Section 4 we use L_1 trend filtering to estimate the fluctuations in the Lyman-alpha forest absorption field embedded in the spectra of high redshift quasars observed by BOSS.

2 L_1 TREND FILTERING

Suppose we observe noisy measurements of a response variable of interest (e.g. flux, magnitude, photon counts) according to the data generating process (DGP)

$$f(t_i) = f_0(t_i) + \epsilon_i, \quad (1)$$

where the one-dimensional inputs t_1, \dots, t_n are not necessarily equally-spaced and $\epsilon_1, \dots, \epsilon_n$ are measurement errors with $\mathbb{E}[\epsilon_i] = 0$ (where we use $\mathbb{E}[\cdot]$ to denote mathematical expectation). If measurement variances $\text{Var}(\epsilon_i) = \sigma_i^2$, $i = 1, \dots, n$ are known or estimates are available, they can be used to improve the estimator by weighting the data points in the fitting criterion below—Equation (2). If estimates are not available then we take the points to be equally weighted.

2.1 Definition of the estimator

For any integer-valued polynomial order $k \geq 0$ and tuning parameter $\gamma > 0$, the (discrete) k th order L_1 trend filter $\hat{f}(\gamma, k) = (\hat{f}(t_1; \gamma, k), \dots, \hat{f}(t_n; \gamma, k))^T$ is defined as the minimizer of the following penalized weighted sum of squared error:

$$\hat{f}(\gamma, k) = \arg \min_{g \in \mathbb{R}^n} \|W(f - g)\|_2^2 + \gamma \|D^{(t, k+1)} g\|_1, \quad (2)$$

where $f = (f(t_1), \dots, f(t_n))^T$ is the vector of observed responses, $W = \text{diag}(\sigma_1^{-1}, \dots, \sigma_n^{-1})$ is a weighting matrix, $D^{(t, k+1)}$ is the discrete difference operator of order $k + 1$, and $\|\cdot\|_p$, $p = 1, 2$ is the L_p norm

$$\|f\|_p = \left(\sum_{i=1}^n |f(t_i)|^p \right)^{1/p}. \quad (3)$$

When $k = 0$, we have

$$D^{(t, 1)} = \begin{bmatrix} 1 & -1 & 0 & \cdots & 0 & 0 \\ 0 & 1 & -1 & \cdots & 0 & 0 \\ \vdots & & & & & \\ 0 & 0 & 0 & \cdots & 1 & -1 \end{bmatrix} \in \mathbb{R}^{(n-1) \times n}, \quad (4)$$

and

$$\|D^{(t, 1)} g\|_1 = \sum_{i=1}^{n-1} |g(t_i) - g(t_{i+1})|. \quad (5)$$

In this case, \hat{f} has a piecewise constant structure with the adaptively chosen knots corresponding to the nonzero entries in

$$D^{(t, 1)} \hat{f} = (\hat{f}(t_2; \gamma) - \hat{f}(t_1; \gamma), \dots, \hat{f}(t_n; \gamma) - \hat{f}(t_{n-1}; \gamma)). \quad (6)$$

Therefore, 0th order L_1 trend filtering is the same as one-dimensional total variation denoising (Rudin et al. 1992) and the one-dimensional fused lasso (Tibshirani et al. 2005) with solely the fusion penalty. For $k \geq 1$ the difference operator can be recursively defined as

$$D^{(t, k+1)} = D^{(1)} V D^{(t, k)} \quad (7)$$

where

$$D^{(1)} = \begin{bmatrix} 1 & -1 & 0 & \cdots & 0 & 0 \\ 0 & 1 & -1 & \cdots & 0 & 0 \\ \vdots & & & & & \\ 0 & 0 & 0 & \cdots & 1 & -1 \end{bmatrix} \in \mathbb{R}^{(n-k-1) \times (n-k)}, \quad (8)$$

and

$$V = \text{diag} \left(\frac{k}{t_{k+1} - t_1}, \frac{k}{t_{k+2} - t_2}, \dots, \frac{k}{t_n - t_{n-k}} \right). \quad (9)$$

In the case of unit input spacing, $D^{(t, k+1)}$, $k = 0, 1, 2$ simplify to

$$D^{(t, 1)} = \begin{bmatrix} 1 & -1 & 0 & \cdots & 0 & 0 \\ 0 & 1 & -1 & \cdots & 0 & 0 \\ \vdots & & & & & \\ 0 & 0 & 0 & \cdots & 1 & -1 \end{bmatrix} \in \mathbb{R}^{(n-1) \times n}, \quad (10)$$

$$D^{(t, 2)} = \begin{bmatrix} 1 & -2 & 1 & 0 & \cdots & 0 \\ 0 & 1 & -2 & 1 & \cdots & 0 \\ 0 & 0 & 1 & -2 & \cdots & 0 \\ \vdots & & & & & \end{bmatrix} \in \mathbb{R}^{(n-2) \times n}, \quad (11)$$

$$D^{(t, 3)} = \begin{bmatrix} 1 & -3 & 3 & -1 & \cdots & 0 \\ 0 & 1 & -3 & 3 & \cdots & 0 \\ 0 & 0 & 1 & -3 & \cdots & 0 \\ \vdots & & & & & \end{bmatrix} \in \mathbb{R}^{(n-3) \times n}, \quad (12)$$

respectively. The criterion (2) is strictly convex for all k and can be solved by various convex optimization algorithms in nearly linear time (Kim et al. 2009; Tibshirani & Taylor 2011; Arnold & Tibshirani 2016; Ramdas & Tibshirani 2016). The strict convexity of (2) guarantees a unique solution for all orders $k \geq 0$, however algorithms can become unstable for $k \geq 3$. Therefore, we limit our discussion in this work to $k \in \{0, 1, 2\}$ and do not recommend the use of $k \geq 3$. Figure 1 exhibits the L_1 trend filtered estimates of orders $k = 0, 1, 2$ on a mock quasar Lyman-alpha forest from Bautista et al. (2015), with the tuning parameter γ optimally chosen on each (detailed in Section 2.2). Tick marks indicate the locations of the adaptively chosen knots of each piecewise polynomial. In this example, the most prominent symptom of spatial heterogeneity is the occasional abrupt dip in the

³ http://stanford.edu/~boyd/l1_tf

⁴ <https://github.com/joshloyal/L1-Trend-Filtering>

⁵ <https://github.com/hadley/l1tf>

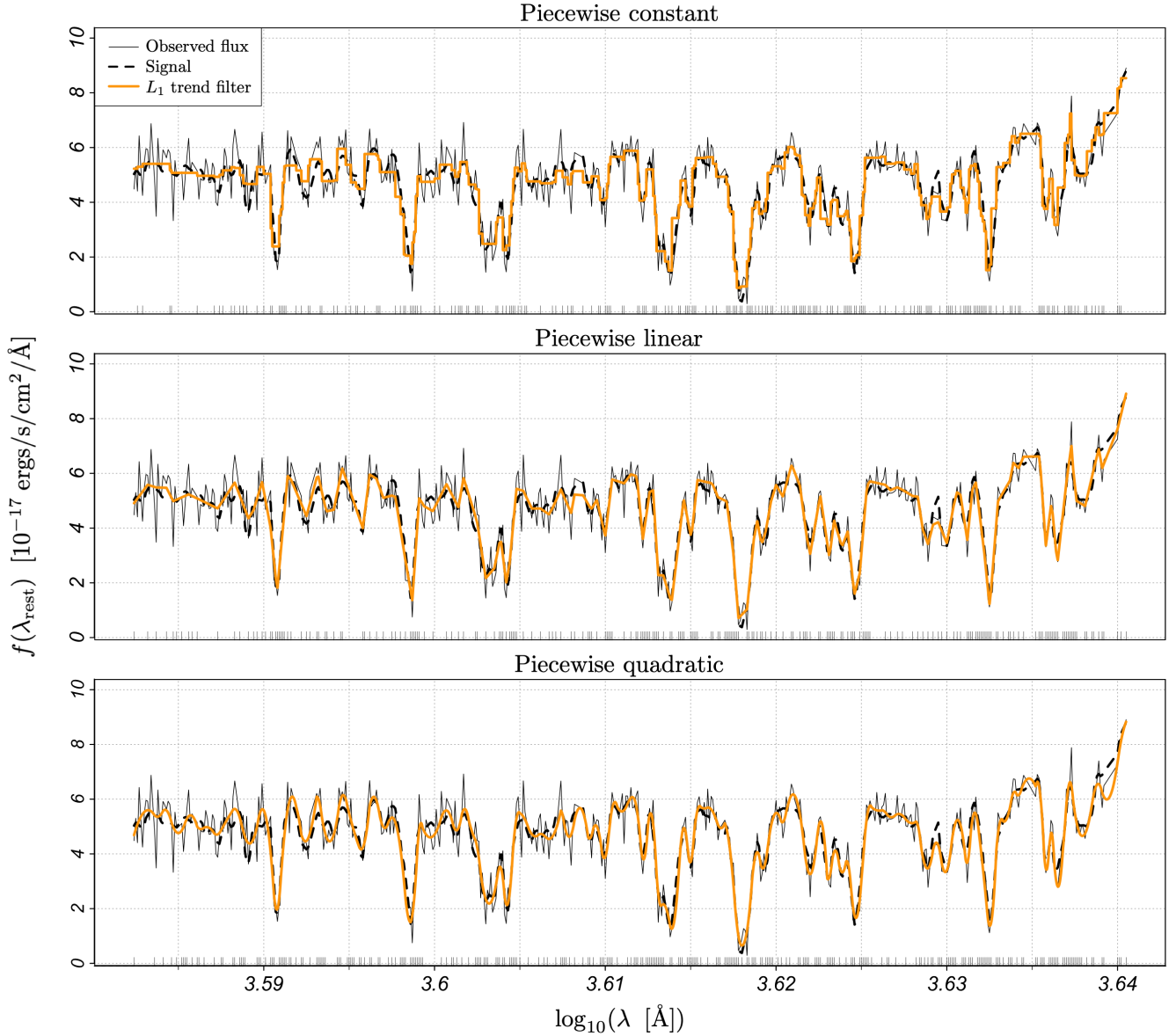


Figure 1. Lyman-alpha forest of a mock quasar spectrum (Bautista et al. 2015) in logarithmic-angstrom space with L_1 trend filtered estimates. From top to bottom, we show the L_1 trend filter for orders $k = 0, 1$, and 2 , which take the form of piecewise constant, piecewise linear, and piecewise quadratic polynomials, respectively. The adaptively chosen knots of each piecewise polynomial are indicated by the tick marks along the x -axis. The piecewise constant L_1 trend filter is discontinuous, but we interpolate here for visual purposes.

signal caused by an over-density of absorbing neutral hydrogen in the intergalactic medium. We study this application in detail in Section 4.

2.2 Tuning the complexity

The choice of the piecewise polynomial order k generally has minimal effect on the performance of the estimator in terms of mean-squared error (MSE) and thus can be treated as a heuristic choice. In this work we use $k = 2$ as our default choice. Given k , the parameter $\gamma > 0$ is used to tune the complexity (i.e. the wiggleness) of the L_1 trend filter by weighting the tradeoff between the smoothness of \hat{f} and the size of the squared residuals. Therefore, obtaining an accurate estima-

tor is intrinsically tied to finding an optimal balance in this tradeoff. The selection of γ is typically done by minimizing an estimate of the out-of-sample error. Here, there are two different notions of error to consider, namely, *fixed-input* error and *random-input* error. As the names suggest, the distinction between which type of error to use is made based on how the inputs are sampled. As a general rule-of-thumb, we recommend optimizing with respect to fixed-input error when the inputs are regularly-sampled and optimizing with respect to random-input error on irregularly-sampled data.

Let \mathcal{Q} denote the DGP stated in (1). The fixed-input

error is given by

$$R(\gamma) = \sum_{i=1}^n \mathbb{E}_Q \left[(f(t_i) - \hat{f}(t_i; \gamma))^2 \mid t_1, \dots, t_n \right] \quad (13)$$

$$= \sum_{i=1}^n \mathbb{E}_Q \left[(f_0(t_i) - \hat{f}(t_i; \gamma))^2 \mid t_1, \dots, t_n \right] + \sigma_i^2 \quad (14)$$

and the random-input error is given by

$$\tilde{R}(\gamma) = \mathbb{E}_Q \left[(f(t) - \hat{f}(t; \gamma))^2 \right], \quad (15)$$

where, in the latter, t is considered to be a random component of the DGP. In each case, the optimal choice of γ is defined as the minimizer of the respective choice of error. Empirically, we estimate the optimal choice of γ by minimizing an estimate of (13) or (15). For fixed-input error we recommend Mallows' C_p estimator (Mallows 1973) and for random-input error we recommend K -fold cross validation with $K = 10$. We elaborate on Mallows' C_p here and refer the reader to Hastie et al. (2001) for K -fold cross validation. The following formula is a generalization of Mallows' C_p estimator (Efron 1986; 2004) that provides an unbiased estimate of the fixed-input error of a general regression estimator

$$\hat{R}_0(\gamma) = \frac{1}{n} \sum_{i=1}^n (f(t_i) - \hat{f}(t_i; \gamma))^2 + \frac{2}{n} \sum_{i=1}^n \text{Cov}(\hat{f}(t_i), f(t_i)) \quad (16)$$

$$= \frac{1}{n} \sum_{i=1}^n (f(t_i) - \hat{f}(t_i; \gamma))^2 + \frac{2\bar{\sigma}^2 \text{df}(\hat{f})}{n}, \quad (17)$$

where $\bar{\sigma}^2 = n^{-1} \sum_{i=1}^n \sigma_i^2$ and $\text{df}(\hat{f}) = \bar{\sigma}^{-2} \sum_{i=1}^n \text{Cov}(\hat{f}(t_i), f(t_i))$ is a measure of the complexity of \hat{f} known as the *effective degrees of freedom*. A formula for the effective degrees of freedom of the L_1 trend filter is available via the generalized lasso results of Tibshirani & Taylor (2012). Namely,

$$\text{df}(\hat{f}) = \mathbb{E}[\text{number of knots in } \hat{f}] + k + 1 \quad (18)$$

$$= \mathbb{E}[\|D^{(t, k+1)} \hat{f}\|_0] + k + 1, \quad (19)$$

where $\|\cdot\|_0$ is the L_0 norm that counts the number of nonzero elements in $D^{(t, k+1)} \hat{f}$. We then obtain our tuning parameter estimate $\hat{\gamma}$ by minimizing the following plug-in estimate for (16)

$$\hat{R}(\gamma) = \sum_{i=1}^n (f(t_i) - \hat{f}(t_i; \gamma))^2 + \frac{2\hat{\sigma}^2 \text{df}(\hat{f})}{n}, \quad (20)$$

where df is an estimate for the effective degrees of freedom obtained by replacing the expectation in (19) with the observed number of knots and $\hat{\sigma}^2$ is an estimate of $\bar{\sigma}^2$. If a reliable estimate of $\bar{\sigma}^2$ is not available, a data-driven estimate can be constructed (see, for example, Wasserman 2006). We provide R code on the corresponding author's Github page⁶ for implementing Mallows' C_p with L_1 trend filtering. The code is built on top of the `glmgen` R package of Ramdas & Tibshirani (2016), which already includes an implementation for K -fold cross validation.

⁶ <https://github.com/capolitsch>

3 APPLICATIONS

As previously stated, the defining property of an application for which L_1 trend filtering is especially useful is when the signal possesses mixed degrees of smoothness, i.e. spatial heterogeneity. We emphasize *especially useful* here because the performance of the L_1 trend filter on spatially heterogeneous signals is what sets it apart from classical methods. The L_1 trend filter is also statistically optimal for estimation of spatially homogeneous signals, but this property is widely held by classical methods.

The estimation of spatially heterogeneous signals is a pervasive problem in time-domain astronomy and astronomical spectroscopy, and naturally we can only demonstrate a small set of examples here. The data sets we briefly examine in this section are two Kepler light curves, a Palomar Transient Factory (PTF) supernova light curve, and a Sloan Digital Sky Survey (SDSS) galaxy spectrum.

3.1 Kepler light curves

NASA's Kepler and K2 missions (Borucki et al. 2010; Howell et al. 2014) naturally come to mind in the discussion of analyzing heterogeneous signals in the time domain. Over nearly a decade of collection starting in March of 2009, the Kepler space telescope collected high precision light curves for over 500,000 stars. In Figure 2, we show phase-folded light curves for two Kepler star systems: Kepler-10 (a confirmed exoplanet host; Batalha et al. 2011) and KIC 6387887 (an eclipsing binary star system). We superpose an L_1 trend filter on each, with the tuning parameter chosen by K -fold cross validation.

Kepler-10 is confirmed to host at least two exoplanets, with each detected using the transit method—a measurable periodic dimming in the photometry caused by the planet crossing in front of the star. The light curve shown in Figure 2 is phased to the 45.29 day orbital period of the star's second confirmed planet—Kepler-10 c (KIC 11904151 c; Fressin et al. 2011). A transit light curve signal characteristically exhibits a relatively constant or smoothly changing intensity that is periodically interrupted by a short abrupt dip at each transit event.

Statistically, an eclipsing binary system exhibits a similar type of light curve signal to the exoplanet transit. An eclipsing binary light curve is characterized by two deep dips per phase—corresponding to a primary and secondary eclipse of the binary system—among an otherwise smoothly varying signal. The primary eclipse corresponds to the deeper dip in brightness, and is positioned at **Phase** = 0 in the bottom panel of Figure 2. The L_1 trend filter is a convenient alternative, both computationally and statistically, to the Kepler `polyfit` model—a chain of four polynomials with knots selected by eye or an iterative computational search (Prša et al. 2008).

3.2 PTF supernova light curve

Figure 3 shows a UVM2-band light curve for the Type Ia supernova SN2011fe (Nugent et al. 2011; also known as PTF11kly), with an L_1 trend filter tuned by K -fold cross validation. SN2011fe was discovered on August 24, 2011 by the PTF survey (Law et al. 2009) using the 1.2-m Oschin

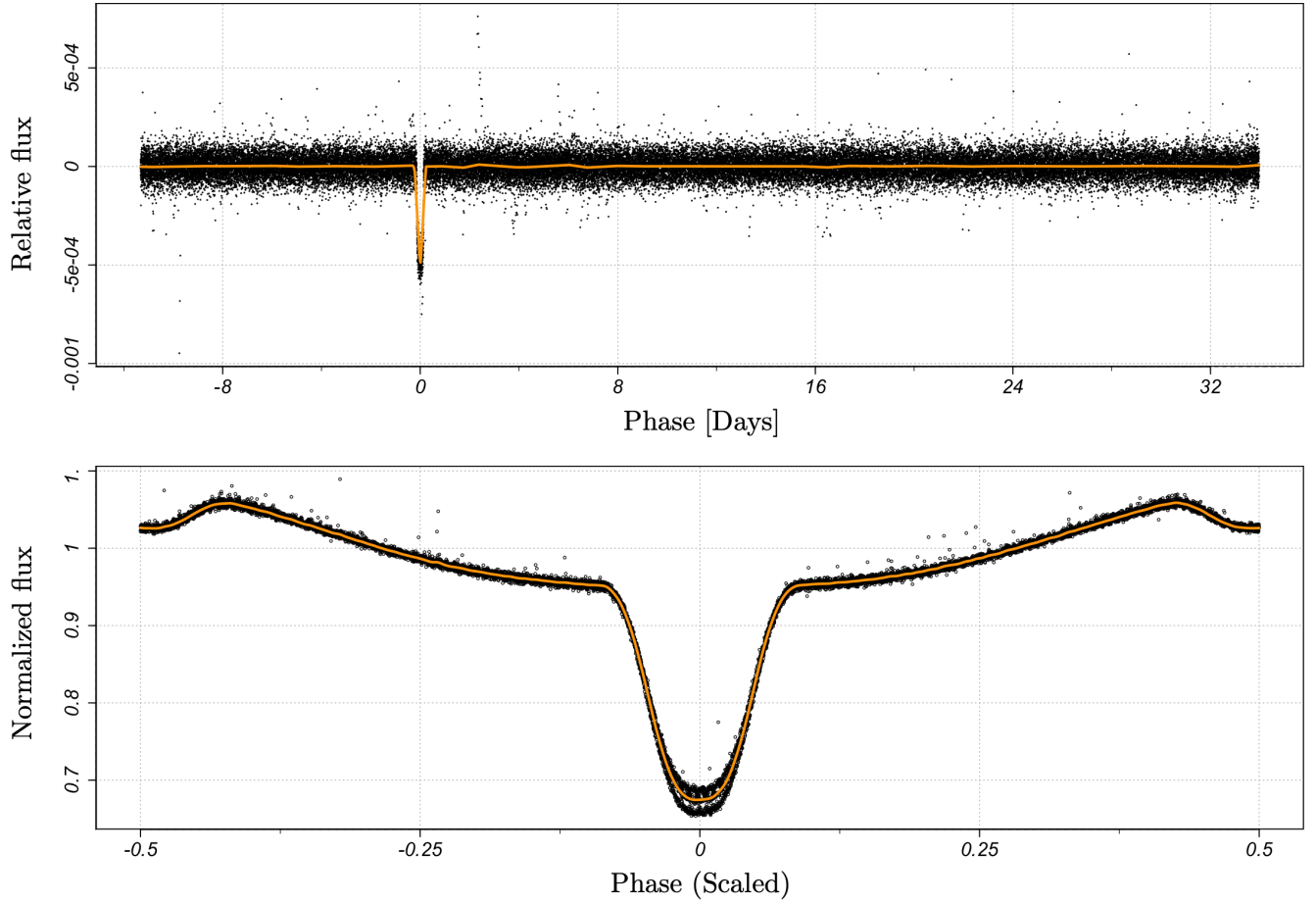


Figure 2. Two phase-folded Kepler light curves with L_1 trend filter superposed, tuned by K -fold cross validation. **Top:** Photometry for Kepler-10, folded based on the orbital period of the exoplanet Kepler-10 c (KIC 11904151 c; [Fressin et al. 2011](#)). The L_1 trend filter captures the (abrupt) exoplanet transit event (defined to be **Phase** = 0), and remains stable throughout the rest of the orbital phase. **Bottom:** Photometry for a Kepler eclipsing binary star system (KIC 6387887). The primary eclipse (centered at **Phase** = 0) creates a deep dip in luminosity among an otherwise relatively smooth light curve. Here, the L_1 trend filter provides an efficient alternative (both computationally and statistically) to the Kepler `polyfit` estimate.

Schmidt Telescope at Palomar Observatory and was located in the Pinwheel Galaxy (M101) approximately 6.4 Mpc from Earth. The initial very rapid increase to the maximum luminosity (here on September 10, 2011), followed by a sharp decrease and increasingly smooth decay is characteristic of a Type Ia supernova.

3.3 SDSS galaxy spectrum

Figure 4 shows the electromagnetic spectrum of a galaxy in the northern galactic cap at redshift $z \approx 0.232$. The spectrum comes from the twelfth data release of the Baryon Oscillation Spectroscopic Survey (BOSS DR12; [Alam et al. 2015](#)), operating within the third phase of the Sloan Digital Sky Survey (SDSS-III; [Aihara et al. 2011](#)). The L_1 trend filter is fit in the logarithmic-angstrom wavelength space in which the observations are equally spaced, and the complexity is chosen by minimizing Mallows' C_p . The signal exhibits intervals of relative smoothness coupled with localized small-scale features such as emission peaks and absorption lines.

4 APPLICATION TO QUASAR LYMAN-ALPHA FOREST

In this section we study another spectroscopic application in more detail. In particular, we study the Lyman-alpha ($\text{Ly}\alpha$) forest of quasars — an absorption phenomenon that appears in the restframe wavelength range $(\lambda_{\text{Ly}\beta}, \lambda_{\text{Ly}\alpha}) = (1025.72 \text{ \AA}, 1215.67 \text{ \AA})$ due to the presence of electrically neutral hydrogen (H I) in the intergalactic medium (IGM). The relative fluctuations in the $\text{Ly}\alpha$ forest transmitted flux fraction are of primary interest since they possess a monotonic relationship with the relative distribution of the absorbing H I. At redshifts $z < 5$, the probability density function of the absorption field is highly negatively skewed, which leads to a spatially heterogeneous absorption trend in the spectrum of the background quasar, characterized by abrupt intermittent dips in the quasar flux (see Figure 1) that correspond to high H I density regions. To a lesser degree, spatial heterogeneity also arises as a result of the $(1+z)$ redshift factor that stretches the absorptions along the line of sight to a quasar.

As in the galaxy spectrum example in Section 3.3, we

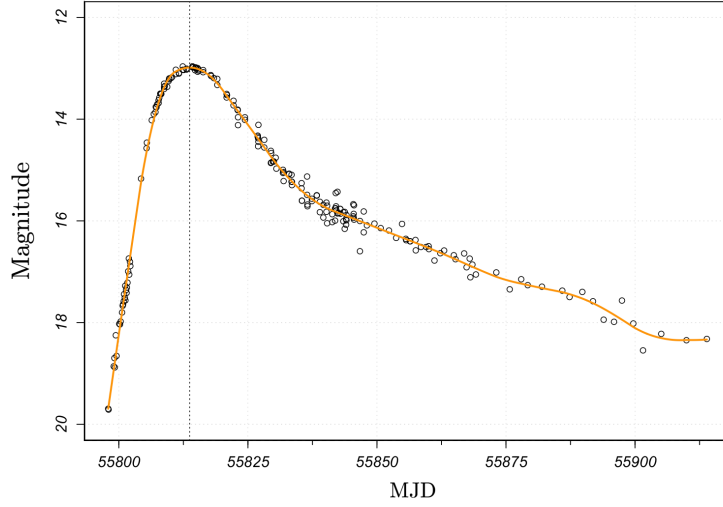


Figure 3. UVM2-band photometry for the Type Ia supernova SN2011fe (Nugent et al. 2011; also known as PTF11kly) discovered on August 24, 2011, located in the Pinwheel Galaxy (M101) in the constellation Ursa Major, approximately 6.4 Mpc from Earth. Characteristically, the light curve exhibits an initial very rapid increase to the peak brightness (dotted line) followed by an increasingly smooth decline, which is captured well by the L_1 trend filter (orange line).

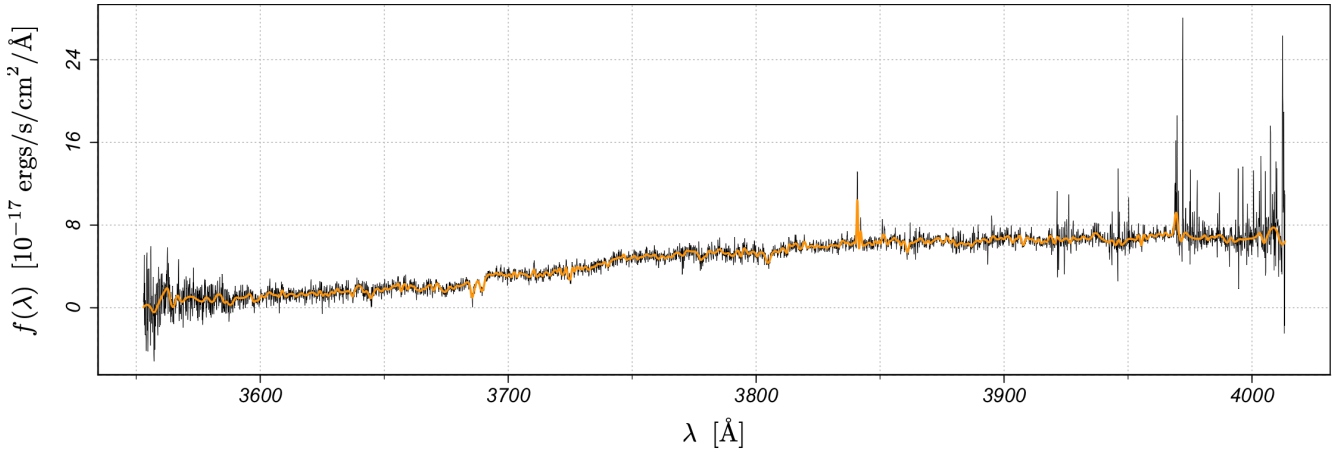


Figure 4. Spectrum of a galaxy located at (RA, Dec, z) \approx (237.690°, 2.162°, 0.232), collected by the Baryon Oscillation Spectroscopic Survey (Alam et al. 2015; Plate = 4055, MJD = 55359, Fiber = 18) of the third phase of the Sloan Digital Sky Survey (Aihara et al. 2011), with the L_1 trend filter shown in orange. The L_1 trend filter is fit in the logarithmic wavelength space in which the observations are equally spaced, and the complexity is chosen by minimizing Mallows' Cp estimator of fixed-input error.

use the L_1 trend filter to extract the spatially heterogeneous flux signal in an observed spectrum — but, here, only in the Ly α forest. Estimates for the fluctuations in transmitted flux due to absorbing H I then follow by coupling the denoised Ly α forest with estimates for the quasar continuum and the cosmic mean transmitted flux in the Ly α forest. Alternatively, the mean flux level — defined as the product of the continuum and cosmic mean transmitted flux — can be estimated directly, as in Croft et al. (2002), and we follow this approach. The mean flux level is a very smooth, spatially homogeneous function within the truncated Ly α forest restframe. It is therefore appropriate to use a classical nonparametric method for this stage of estimation. Specifically, we use local polynomial regression (LPR; Cleveland 1979; Fan & Gijbels 1996; Loader 1999). We illustrate the

methods on a mock quasar Ly α forest from Bautista et al. (2015) and a real quasar Ly α forest from BOSS DR12.

4.1 Notation

Suppose we observe a quasar located at redshift $z = z_0$. The observational DGP of the Ly α forest can be assumed to follow the model

$$f(\lambda) = f_0(\lambda) + \epsilon(\lambda), \quad \lambda \in \Lambda(z_0), \quad (21)$$

$$= \bar{F}(\lambda) \cdot C(\lambda) \cdot (1 + \delta_F(\lambda)) + \epsilon(\lambda), \quad (22)$$

where $f(\lambda)$ is the observed flux at wavelength λ , $f_0(\lambda)$ is the signal (taken to be fixed), $\epsilon(\lambda)$ is zero mean white Gaussian noise, $\Lambda(z_0) = (\lambda_{Ly\beta}, \lambda_{Ly\alpha}) \cdot (1 + z_0)$ is the redshifted Ly α

Input	Definition	Range (quasar at $z = z_0$)
λ	Observed wavelength	$\bar{\Lambda}(z_0)$
ν	Rest wavelength	$\bar{\Lambda}_{\text{rest}}(z_0) = \bar{\Lambda}(z_0)/(1 + z_0)$
z	Redshift	$\Pi(z_0) = \bar{\Lambda}(z_0)/\lambda_{\text{Ly}\alpha} - 1$
ζ	Logarithmic wavelength (scaled)	$Z(z_0) = 10^4 \cdot \log_{10}(\bar{\Lambda}(z_0))$

Table 1. Various input spaces utilized for the Ly α forest analysis. Notation of functions is held constant, e.g. $\delta_F(\cdot)$, and an alteration of the input variable is understood as a change of input spaces. Logarithmic wavelengths are scaled for numerical stability of the optimization algorithm.

forest, $C(\lambda)$ is the flux of the unabsorbed quasar continuum, $F(\lambda) = f_0(\lambda)/C(\lambda)$ is the transmitted flux fraction, $\bar{F}(\lambda) = \mathbb{E}[F(\lambda)]$ is the mean transmitted flux fraction (over the sky) in the Ly α forest at redshift $z = \lambda/\lambda_{\text{Ly}\alpha} - 1$, and

$$\delta_F(\lambda) = F(\lambda)/\bar{F}(\lambda) - 1 \quad (23)$$

is the fluctuation about the mean Ly α transmitted flux at redshift $z = \lambda/\lambda_{\text{Ly}\alpha} - 1$. Here, δ_F is the quantity we are primarily interested in estimating since $\delta_F \propto \delta_{\text{HI}}^{-1}$ at each fixed redshift, where δ_{HI} is the density of H I. The estimation of the flux signal f_0 is viewed as an ancillary step.

Although, in principle, it is preferable to study the full spectral range $\Lambda(z_0)$ we have found that, in the nonparametric setting, estimating the quasar continuum near the localized Ly α and Ly β emission peaks at the boundaries of the forest reduces the estimation accuracy in the interior of $\Lambda(z_0)$. Therefore, in this work we limit our analysis to the truncated Ly α forest range

$$\bar{\Lambda}(z_0) = (1045 \text{ \AA}, 1195 \text{ \AA}) \cdot (1 + z_0). \quad (24)$$

We simplify notation in this work by changing the input space of the functions introduced above by merely altering the input variable. For example, regarding the quantity δ_F , we maintain the notation $\delta_F(\lambda)$, $\delta_F(\lambda_{\text{rest}})$, $\delta_F(z)$, and $\delta_F(\zeta)$, while it is understood that a proper change of input spaces has taken place. The various input spaces are defined in Table 1.

4.2 L_1 trend filter

We use the L_1 trend filter to estimate the flux signal f_0 of the observational model (21). In both BOSS DR12 and the Bautista et al. (2015) mock catalog, the spectra are sampled on equally-spaced grids in logarithmic wavelength space with $\Delta \log_{10}(\lambda_i) = 10^{-4}$ dex (in logarithmic angstroms) and flux measurement variances are provided by the BOSS pipeline (Bolton et al. 2012) — accounting for the statistical uncertainty introduced by photon noise, CCD read noise, and sky-subtraction error. We correct the BOSS spectrum for interstellar extinction with the Cardelli et al. (1989) extinction law and the Schlafly & Finkbeiner (2011) dust map.

We fit the L_1 trend filter on the equally-spaced logarithmic grid and tune the complexity by minimizing Mallows' C_p estimate of the fixed-input mean-squared error (MSE). More precisely, we fit the L_1 trend filter in the space $Z(z_0) = 10^4 \cdot \log_{10}(\bar{\Lambda}(z_0))$, as defined in Table 1, where we add the scaling to unit spacing for numerical stability of the convex optimization.

4.3 Nonparametric continuum estimation

We utilize a modified Croft et al. (2002) approach to propagate the L_1 trend filtered estimates for the flux signal f_0 from Section 4.2 into estimates for the fluctuation field δ_F along a line of sight to an observed quasar. Namely, given the L_1 trend filter \hat{f} , we directly estimate the smooth mean flux level defined by the product $m = \bar{F} \cdot C$ and then define the δ_F estimates as the ratio $\hat{\delta}_F := \hat{f}/\hat{m} - 1$. We carry out the estimation of m via a wide-kernel LPR on the L_1 trend filtered estimates, with the specific bandwidth of the kernel selected by optimizing over a large sample of mock spectra (detailed in Section 4.4). We find that regressing on the denoised estimates—instead of the observational DGP (21)—significantly improves the accuracy and robustness of the δ_F estimates. We carry out the LPR estimation in the Ly α restframe $\bar{\Lambda}_{\text{rest}}(z_0)$ (see Table 1) in order to remove the effect of redshifting on the smoothness of m . The LPR estimation of m is a fully nonparametric procedure and provides a reduction in bias over popular parametric approaches such as low-order power laws and principal components analyses (PCA). The sole assumption of the LPR estimator is that, in the restframe, the mean flux level m always has a fixed degree of smoothness, as defined by the optimal choice of kernel bandwidth.

To be explicit, the LPR estimator for m is a regression on the data set

$$\{(v_i, \hat{f}(v_i; \hat{\gamma}))_{i=1}^n, \quad v_i \in \bar{\Lambda}_{\text{rest}}(z_0), \quad (25)$$

which can be viewed as arising from the DGP

$$\hat{f}(v_i; \hat{\gamma}) = m(v_i) + \rho_i, \quad (26)$$

where \hat{f} is the L_1 trend filter fixed at the minimum Mallows' C_p tuning parameter $\hat{\gamma}$, $e_i = \hat{f}(v_i; \hat{\gamma}) - f_0(v_i)$ are the errors of the L_1 trend filter, and $\rho_i = m(v_i) \cdot \delta_F(v_i) + e_i$ are autocorrelated fluctuations about zero. The LPR estimator is the natural extension of kernel regression (Nadaraya 1964; Watson 1964) to higher-order local polynomials. Given a kernel function $K(\cdot)$ with bandwidth $h > 0$, for each $i = 1, \dots, n$, the LPR estimator is obtained by minimizing

$$\sum_{j=1}^n \left(\hat{f}(v_j; \hat{\gamma}) - P_{v_i}(v_j; \beta_0, \dots, \beta_d) \right)^2 K\left(\frac{|v_j - v_i|}{h}\right), \quad (27)$$

and letting $\hat{m}(v_i) = \hat{\beta}_0$, where $P_{v_i}(\cdot; \beta_0, \dots, \beta_d)$ is a d th order polynomial centered at v_i . Specifically, we utilize the local linear regression estimator (LLR; $d = 1$) and the Epanechnikov kernel (Epanechnikov 1967)

$$K(x) = \frac{3}{4}(1 - x^2)\mathbb{1}_{\{|x| < 1\}}. \quad (28)$$

The LLR estimator is described in full detail by Algorithm 1. Given the L_1 trend filter \hat{f} and the LLR estimate \hat{m} , the δ_F estimates are then defined as

$$\hat{\delta}_F(z_i; \hat{\gamma}) = \frac{\hat{f}(z_i; \hat{\gamma})}{\hat{m}(z_i)} - 1, \quad z_1, \dots, z_n \in \Pi(z_0), \quad (29)$$

where we deliberately express \hat{m} as parameter-less since γ has been fixed at the minimum C_p value $\hat{\gamma}$ and we provide the optimal bandwidth value $h_0 = 74 \text{ \AA}$. Here, we have also done a change of variables to redshift space — the desired domain for studying the H I density fluctuations of the IGM.

Although h_0 is chosen to directly optimize $\hat{\delta}_F$ accuracy,

Algorithm 1 Local polynomial (local linear) estimator for mean flux level

Require: Training Data $\{(v_i, \hat{f}(v_i; \hat{\gamma}))\}_{i=1}^n$, Bandwidth $h_0 = 74 \text{ \AA}$

1: **for all** i **do**

2: Let $\hat{\beta}_0, \hat{\beta}_1$ minimize the locally weighted sum of squares

$$\sum_{j=1}^n \left(\hat{f}(v_j; \hat{\gamma}) - \beta_0 - \beta_1(v_j - v_i) \right)^2 \cdot K \left(\frac{|v_j - v_i|}{h_0} \right).$$

3: Let $\hat{m}(v_i) = \hat{\beta}_0(v_i)$.

4: **end for**

Output: $\{\hat{m}(v_i)\}_{i=1}^n$

an estimator for the quasar continuum $C(\cdot)$ arises intrinsically:

$$\hat{C}(v_i) = \bar{F}(v_i)^{-1} \cdot \hat{m}(v_i), \quad v_i \in \bar{\Lambda}_{\text{rest}}(z_0), \quad (30)$$

where precise estimates of \bar{F} follow from a rich literature (e.g. Bernardi et al. 2003; McDonald et al. 2005; Faucher-Giguère et al. 2008; Dall’Aglio et al. 2009; Pâris et al. 2011; Becker et al. 2013). The δ_F estimates could then be equivalently restated as

$$\hat{\delta}_F(z_i; \hat{\gamma}) = \frac{\hat{F}(z_i; \hat{\gamma})}{\bar{F}(z_i)} - 1, \quad z_1, \dots, z_n \in \Pi(z_0), \quad (31)$$

where

$$\hat{F}(z_i; \hat{\gamma}) = \hat{f}(z_i; \hat{\gamma}) / \hat{C}(z_i). \quad (32)$$

4.4 Calibrating continuum smoothness

We utilize a sample of 124,709 mock quasar spectra from the Bautista et al. (2015) catalog to optimize the bandwidth of the LLR estimator for the mean flux level that intrinsically removes the effect of the quasar continuum. Our mock data reduction is detailed in the Appendix.

For each mock quasar Ly α forest with DGP Q_j , $j = 1, \dots, 124,709$, we first compute the L_1 trend filter tuning parameter that minimizes the *true* fixed-input error

$$\gamma_0^j = \arg \min_{\gamma > 0} \sum_{i=1}^n \mathbb{E}_{Q_j} \left[(f(\zeta_i) - \hat{f}(\zeta_i; \gamma))^2 \mid \zeta_1, \dots, \zeta_n \right]. \quad (33)$$

Then, given the L_1 trend filtered restframe pairs $\{(v_i, \hat{f}(v_i; \gamma_0^j))\}_{i=1}^n$, we fit a LLR estimator with bandwidth h and define the error (as a function of h) of the resulting δ_F estimator as the fixed-input mean absolute deviation (MAD) error

$$R_j(h) = \frac{1}{n} \sum_i \mathbb{E}_{Q_j} \left[|\delta_F(v_i) - \hat{\delta}_F(v_i; \gamma_0^j, h)| \mid v_1, \dots, v_n \right], \quad (34)$$

where \mathbb{E}_{Q_j} denotes the mathematical expectation over the randomness arising from the observational DGP Q_j . Because we can repeatedly sample from each quasar DGP, the expectations in (33) and (34) can be computed to an arbitrary precision. Here, we utilize 300 realizations of each DGP to approximate the expectations.

We then define the optimal choice of h to be the minimizer of the summed error over the full sample of $m = 124,709$

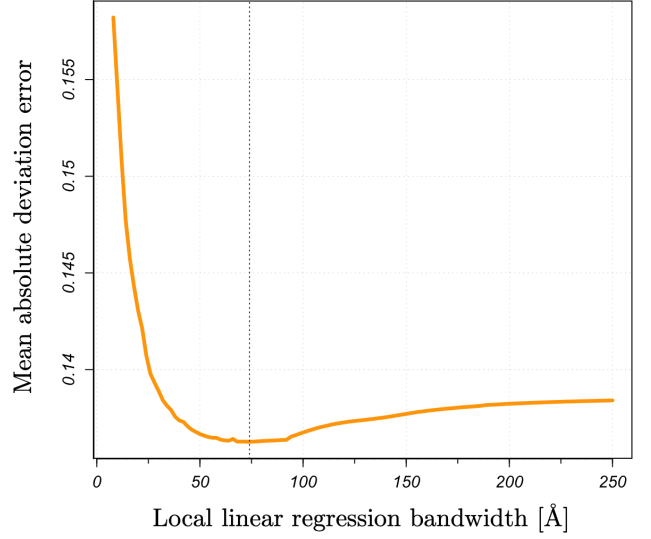


Figure 5. Mean absolute deviation error curve for selecting the optimal bandwidth for the local linear regression estimator for the mean flux level, averaged over the 124,709 spectra in the mock sample. The optimal choice of bandwidth is $h_0 = 74 \text{ \AA}$.

mock quasar spectra

$$h_0 = \arg \min_{h > 0} \sum_{j=1}^m R_j(h). \quad (35)$$

The aggregate error curve is shown in Figure 5, yielding an optimal value of $h_0 = 74 \text{ \AA}$. We find that defining $R(h)$ as the conditional MAD error—instead of the conditional MSE—provides an essential boost in robustness that keeps the error from being dominated by a very small proportion of worst-case estimates.

4.5 Results

The mock quasar Ly α forest from Figure 1 is shown again in Figure 6 with the results of our analysis overlaid. As summarized by the top panel, the L_1 trend filter is fit on the equally-spaced observations in logarithmic wavelength space and then transformed to the restframe wavelength space, where the LLR estimate of the mean flux level is fit. The δ_F estimates are then computed according to (29) and displayed (in redshift space) in the bottom panel, where they can be seen to closely track the true δ_F defined by (23).

An analogous plot is given in Figure 7 for a real quasar Ly α forest from BOSS DR12 (Plate = 6487, MJD = 56362, Fiber = 647). The quasar is located in the northern galactic cap at (RA, Dec, z) \approx (196.680°, 31.078°, 2.560). The estimated δ_F can be interpreted as a proxy for the deviations from the mean H I density in the intervening intergalactic medium at each redshift, with negative values of δ_F corresponding to over-densities of H I and positive values corresponding to under-densities.

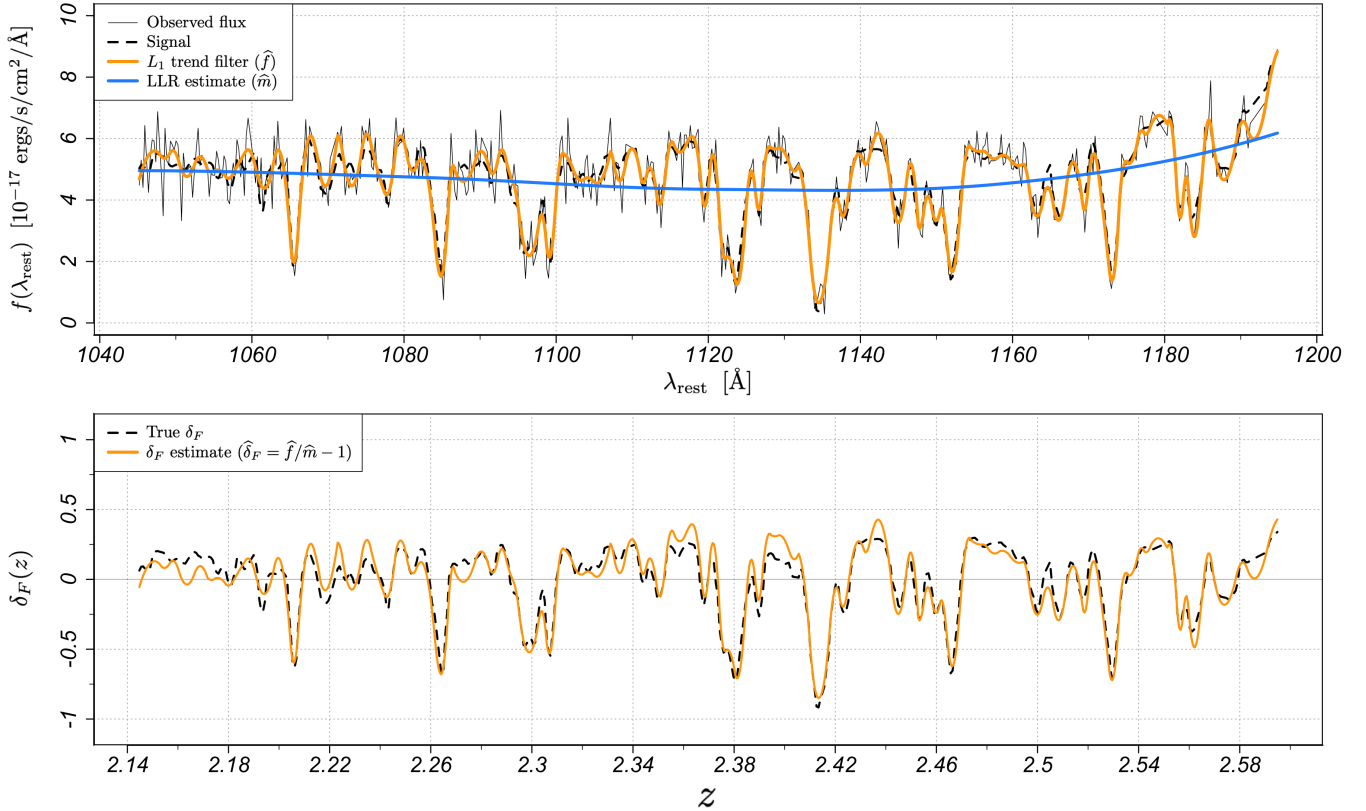


Figure 6. **Top:** Lyman-alpha forest of a mock quasar spectrum (Bautista et al. 2015) in the restframe, with an L_1 trend filter shown in orange and the LLR estimate for the mean flux level shown in blue. **Bottom:** The redshift-space fluctuations in the Lyman-alpha transmitted flux fraction, with our estimate superposed. The fluctuations inversely trace the relative under- and over-densities of neutral hydrogen in the intervening intergalactic medium between Earth and the quasar.

5 SUMMARY

The estimation of one-dimensional spatially heterogeneous signals is central to a wide variety of problems in time-domain astronomy and astronomical spectroscopy, with classical statistical methods largely being ill-suited for the task either due to statistical suboptimality (linear smoothers) or overly-restrictive assumptions (wavelets). L_1 trend filtering is a modern statistical tool that provides statistical optimality for estimating spatially heterogeneous signals without requiring stringent assumptions about the sampling of the data or the behavior of the signal, while also maintaining competitive computational speed. In this work we have demonstrated the performance of L_1 trend filtering on a diverse set of astrophysical data sets: two Kepler light curves (an exoplanet transit and an eclipsing binary system), a Palomar transient Factory supernova light curve, and SDSS galaxy and quasar spectra, with particular detail devoted to the analysis of the Lyman-alpha forest of quasars.

Software for L_1 trend filtering is freely available online across various platforms and we provide links to our recommendations in the footnotes of page 2. Additionally, we make R code available on the corresponding author’s Github

page⁷ for tuning the L_1 trend filtering complexity based on Mallows’ C_p estimate of fixed-input error.

REFERENCES

- Aihara H., et al., 2011, ApJS, 193, 29
- Alam S., et al., 2015, ApJS, 219
- Arnold T. B., Tibshirani R. J., 2016, Journal of Computational and Graphical Statistics, 25, 1
- B. Hall P., et al., 2002, ApJS, 141
- Batalha N. M., et al., 2011, ApJ, 729, 27
- Bautista J. E., et al., 2015, JCAP, 1505
- Becker G. D., Hewett P. C., Worseck G., Prochaska J. X., 2013, MNRAS, 430, 2067
- Bernardi M., et al., 2003, AJ, 125, 32
- Bolton A. S., et al., 2012, AJ, 144, 144
- Borucki W. J., et al., 2010, Science, 327, 977
- Cardelli J., Clayton G., Mathis J., 1989, ApJ, 345, 245
- Cleveland W. S., 1979, Journal of the American Statistical Association, 74, 829
- Croft R. A. C., Weinberg D. H., Katz N., Hernquist L., 1997, ApJ, 488, 532
- Croft R. A., et al., 2002, ApJ, 581
- Dall’Aglio A., Wisotzki L., Worseck G., 2009
- Dawson K., Schlegel D., Ahn C., et al., 2013, AJ, 145, 10

⁷ <https://github.com/capolitsch>

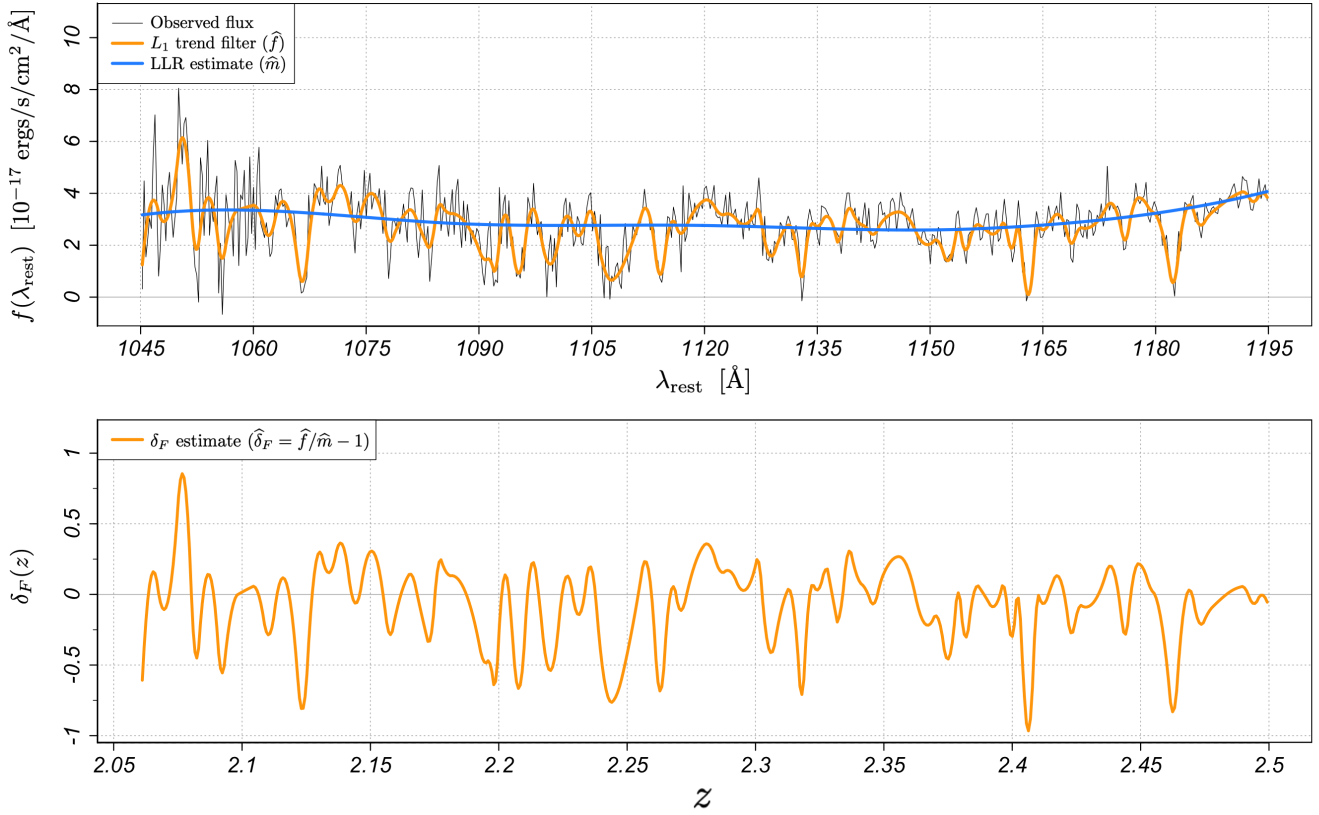


Figure 7. Top: Lyman-alpha forest of a quasar spectrum (in the restframe) from the twelfth data release of the Baryon Oscillation Spectroscopic Survey (Alam et al. 2015; Plate = 6487, MJD = 56362, Fiber = 647). The quasar is located at (RA, Dec, z) \approx (196.680°, 31.078°, 2.560). An L_1 trend filter estimate for the flux signal and a local linear regression estimate for the mean flux level are overlaid. **Bottom:** The estimated relative fluctuations in the Lyman-alpha transmitted flux fraction, due to the presence of absorbing neutral hydrogen in the intergalactic medium (shown in redshift space).

Dhawan S., Leibundgut B., Spyromilio J., Maguire K., 2015, MNRAS, 448, 1345
 Dimitriadis G., et al., 2017, MNRAS, 468, 3798
 Donoho D. L., Johnstone I., 1998, The Annals of Statistics, 26, 879
 Efron B., 1986, Journal of the American Statistical Association, 81, 461
 Efron B., 2004, Journal of the American Statistical Association, 99, 619
 Epanechnikov V., 1967, Theory of Probability & its Applications, 14, 153
 Fan J., Gijbels I., 1996, Local Polynomial Modeling and Its Applications. Chapman and Hall
 Faucher-Giguère C.-A., Lidz A., Hernquist L., Zaldarriaga M., 2008, ApJ, 688, 85
 Fligge M., Solanki S. K., 1997, A&AS, 124, 579
 Francis P. J., Hewett P. C., Foltz C. B., Chaffee F. H., Weymann R. J., Morris S. L., 1991, ApJ, 373, 465
 Fressin F., et al., 2011, ApJS, 197, 5
 Gnedin N. Y., Hui L., 1998, MNRAS, 296, 44
 Golokhov V. Z., Butler N. R., 2014, ApJ, 787, 90
 Hastie T., Tibshirani R., Friedman J., 2001, The Elements of Statistical Learning. Springer Texts in Statistics
 Hellsten U., Hernquist L., Katz N., Weinberg D. H., 1998, ApJ, 499, 172

Howell S. B., et al., 2014, PASP, 126, 398
 Kim S.-J., et al., 2009, SIAM Review, 51, 339
 Law N. M., et al., 2009, PASP, 121, 1395
 Lee K.-G., et al., 2014, ApJL, 795, L12
 Loader C., 1999, Local Regression and Likelihood. Springer-Verlag
 Mallows C. L., 1973, Technometrics, 15, 661
 Mammen E., van de Geer S., 1997, The Annals of Statistics, 25, 387
 Marziani P., Sulentic J. W., Dultzin-Hacyan D., Calvani M., Moles M., 1996, ApJS, 104, 37
 McDonald P., et al., 2005, ApJ, 635, 761
 Nadaraya E. A., 1964, Theory of Probability & its Applications, 9, 141
 Nugent P. E., et al., 2011, Nature, 480, 344
 Osterbrock D. E., Ferland G. J., 2006, Astrophysics of gaseous nebulae and active galactic nuclei
 Palanque-Delabrouille N., et al., 2015, JCAP, 2015, 011
 Pâris I., et al., 2011, A&A, 530
 Peebles M. S., Weinberg D. H., Davé R., Fardal M. A., Katz N., 2010, MNRAS, 404, 1281
 Pieri M. M., Frank S., Weinberg D. H., Mathur S., York D. G., 2010, ApJL, 724, L69
 Prša A., Guinan E. F., Devinney E. J., DeGeorge M., Bradstreet D. H., Giammarco J. M., Alcock C. R., Engle S. G., 2008,

- ApJ, 687, 542
- Ramdas A., Tibshirani R. J., 2016, Journal of Computational and Graphical Statistics, 25, 839
- Rauch M., 1998, ARA&A, 36, 267
- Rudin L. I., Osher S., Fatemi E., 1992, Physica D: Nonlinear Phenomena, 60, 259
- Schlafly E., Finkbeiner D., 2011, ApJ, 737, 103
- Selsing J., Fynbo J. P. U., Christensen L., Krogager J. K., 2016, A&A, 585, A87
- Steidl G., Didas S., Neumann J., 2006, International Journal of Computer Vision, 70, 241
- Tennyson J., 2019, Astronomical Spectroscopy: an Introduction to the Atomic and Molecular Physics of Astronomical Spectroscopy
- Tibshirani R. J., 2014, The Annals of Statistics, 42, 285
- Tibshirani R. J., Taylor J., 2011, The Annals of Statistics, 39, 1335
- Tibshirani R., Taylor J., 2012, The Annals of Statistics, 40, 1198
- Tibshirani R., Saunders M., Rosset S., Zhu J., Knight K., 2005, Journal of the Royal Statistical Society: Series B, 67, 91
- Tolstov A., Nomoto K., Sorokina E., Blinnikov S., Tominaga N., Taniguchi Y., 2019, ApJ, 881, 35
- Wang Y.-X., et al., 2016, Journal of Machine Learning Research, 17, 1
- Wasserman L., 2006, All of Nonparametric Statistics. Springer Texts in Statistics
- Watson G. S., 1964, Sankhyā: The Indian Journal of Statistics, Series A, 26, 359
- York D. G., et al., 2000, AJ, 120, 1579

APPENDIX

Mock data reduction

The mock quasar catalog (Bautista et al. 2015) is designed to mimic the observational data generating processes of the quasar spectra released in Data Release 11 of the Baryon Oscillation Spectroscopic Survey (Alam et al. 2015). We pool the first three realizations of the mock catalog, i.e. M3_0_3/000, M3_0_3/001, and M3_0_3/002 and remove all damped Ly α systems (DLAs), Lyman-limit systems (LLS), and broad absorption line quasars (BALs). We assume no metal absorption in the Ly α forest and correct estimation and subtraction of the sky. We mask all pixels with `and_mask` $\neq 0$ or `or_mask` $\neq 0$. Finally, we retain only the spectra with ≥ 500 pixels in the truncated Ly α forest and those with an optimal L_1 trend filter parameter satisfying $\gamma_0 < 5.25$. Spectra with $\gamma_0 \geq 5.25$ correspond to the very lowest S/N ratio cases, where the L_1 trend filter virtually fits a global constant. The final mock sample contains 124,709 quasar spectra.

This paper has been typeset from a T_EX/L^AT_EX file prepared by the author.